Supplementary Information (SI) for Inorganic Chemistry Frontiers.

Electronic Supplementary Information

Three-dimensional porous rhodium-copper alloy nanoflowers stereoassembled on $Ti_3C_2T_x$ MXene as highly-efficient methanol oxidation electrocatalysts

Haiyan He,[a] Yue Lan,[a] Jinlong Qin,[a] Quanguo Jiang,[a] Lu Yang,[a] Jian Zhang,[b] Huajie Huang*[a]

[a]College of Materials Science and Engineering, Hohai University, Nanjing 210098, China

[b]New Energy Technology Engineering Lab of Jiangsu Province, College of Science, Nanjing University of Posts & Telecommunications (NUPT), Nanjing 210023, China

*E-mail: huanghuajie@hhu.edu.cn

Supplementary Results

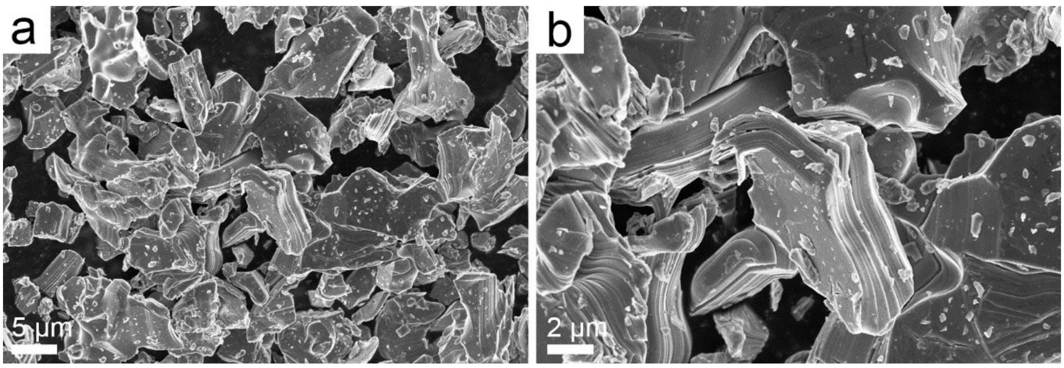

Fig. S1 Representative SEM images of bulk Ti_3AlC_2 at different magnifications.

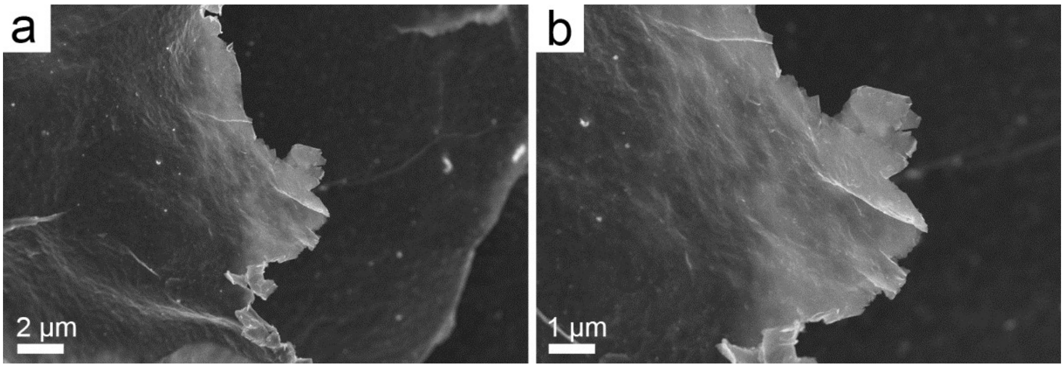

Fig. S2 Representative SEM images of 2D exfoliated $Ti_3C_2T_x$ at different magnifications.

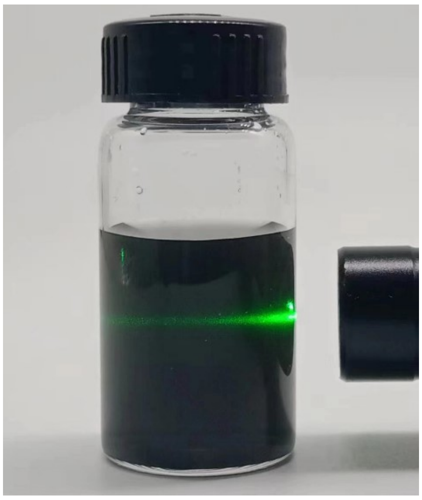

Fig. S3 The Tyndall phenomenon of the as-obtained $Ti_3C_2T_x$ MXene solution

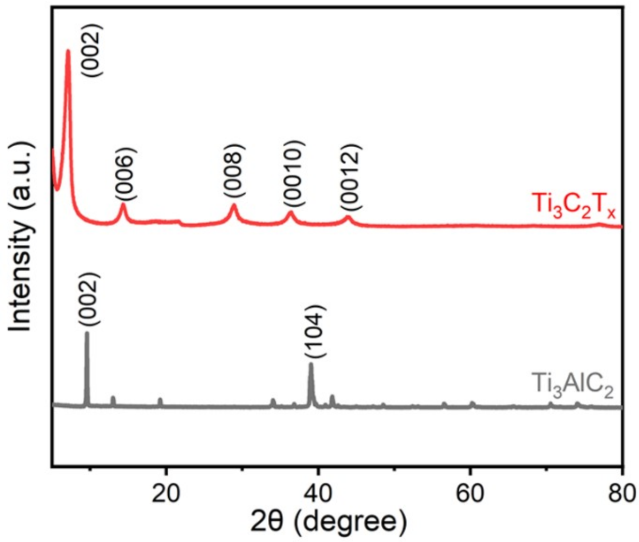

Fig. S4 XRD patterns of the bulk Ti_3AlC_2 and $Ti_3C_2T_x$ nanosheets.

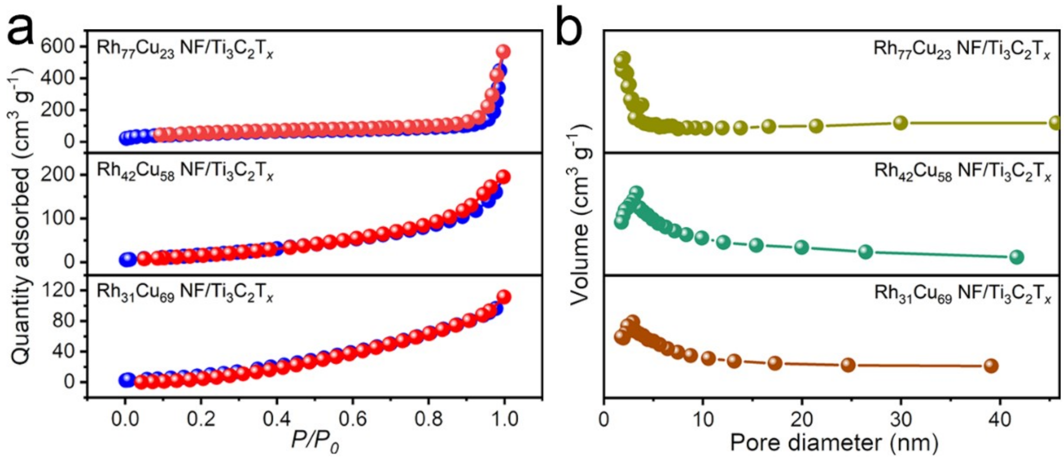

Fig. S5 (a) Nitrogen adsorption-desorption isotherms and (b) pore size distributions of the $Rh_{77}Cu_{23}$ NF/$Ti_3C_2T_x$, $Rh_{42}Cu_{58}$ NF/$Ti_3C_2T_x$ and $Rh_{31}Cu_{69}$ NF/$Ti_3C_2T_x$ samples.

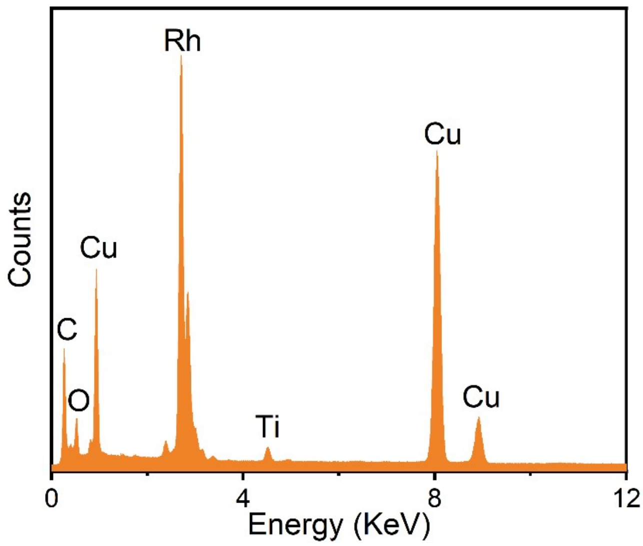

Fig. S6 EDX spectrum of the RhCu NF/$Ti_3C_2T_x$ catalyst.

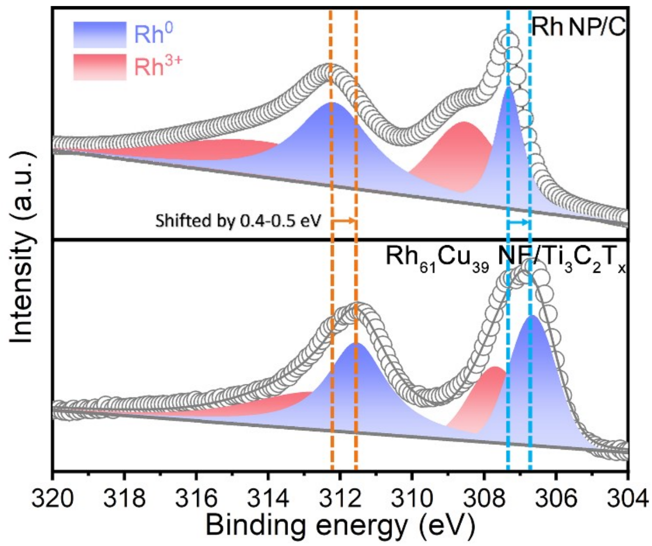

Fig. S7 Comparison of the binding energies for Rh 3*d* spectra of the $Rh_{61}Cu_{39}$ NF/$Ti_3C_2T_x$ and Rh NP/C samples.

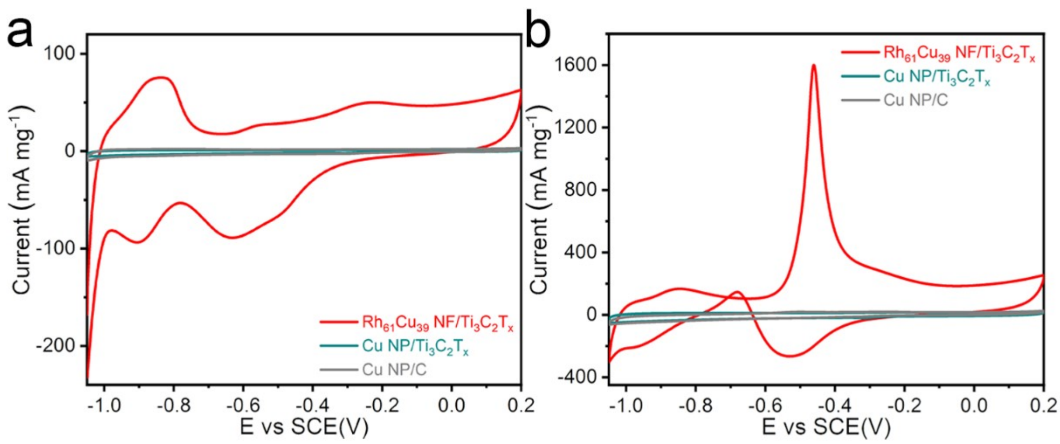

Fig. S8 CV curves of $Rh_{61}Cu_{39}$ NF/$Ti_3C_2T_x$, Cu NP/$Ti_3C_2T_x$ and Cu NP/C in (a) 1 mol L^{-1} KOH and (b) 1 mol L^{-1} KOH with 1 mol L^{-1} CH_3OH solution at 50 mV s^{-1}.

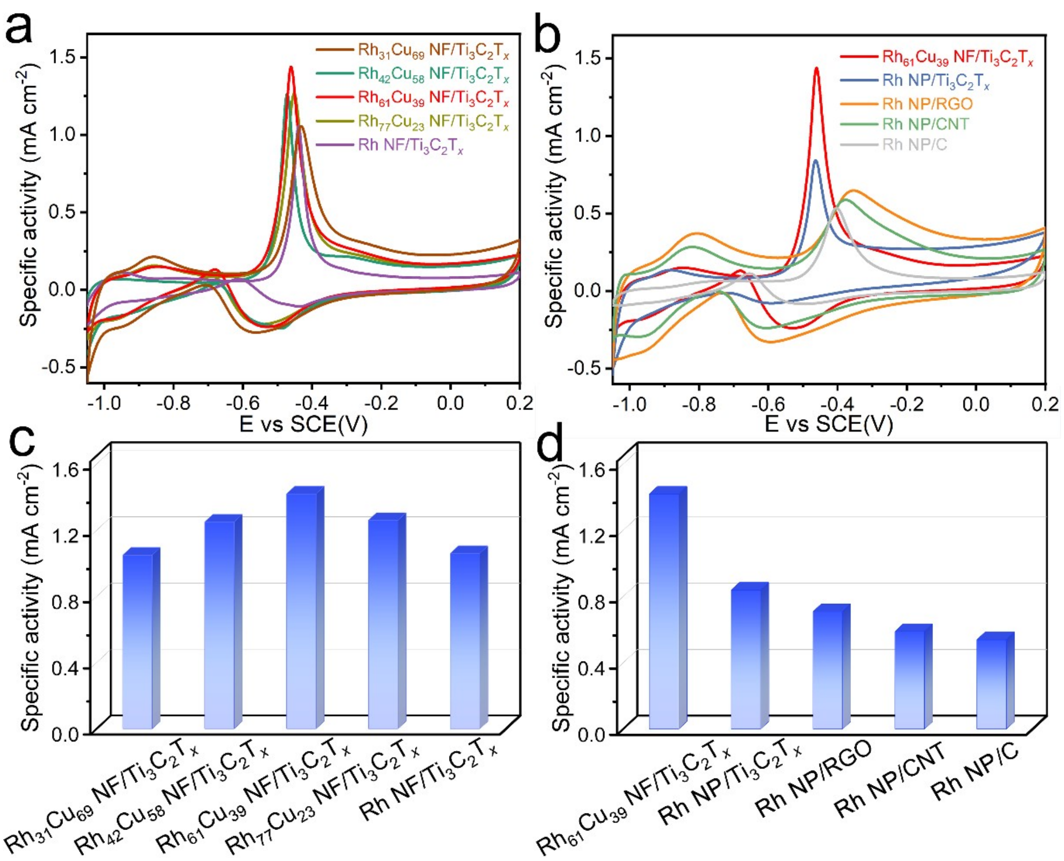

Fig. S9 The ECSA-normalized CV curves of the (a) RhCu NF/$Ti_3C_2T_x$ catalysts with different Rh/Cu ratios and (b) $Rh_{61}Cu_{39}$ NF/$Ti_3C_2T_x$, Rh NP/$Ti_3C_2T_x$, Rh NP/RGO, Rh NP/CNT and Rh NP/C in 1 mol L^{-1} KOH with 1 mol L^{-1} CH_3OH solution. (c-d) Specific activities of various catalysts.

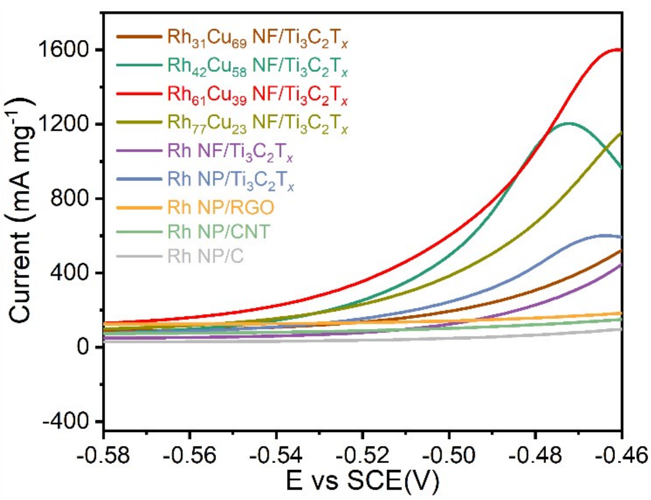

Fig. S10 LSV curves of the RhCu NF/$Ti_3C_2T_x$ electrocatalysts with different Rh/Cu ratios, Rh NP/$Ti_3C_2T_x$, Rh NP/RGO, Rh NP/CNT and Rh NP/C in a 1 mol L^{-1} KOH with 1 mol L^{-1} CH_3OH

solution at 50 mV s^{-1}.

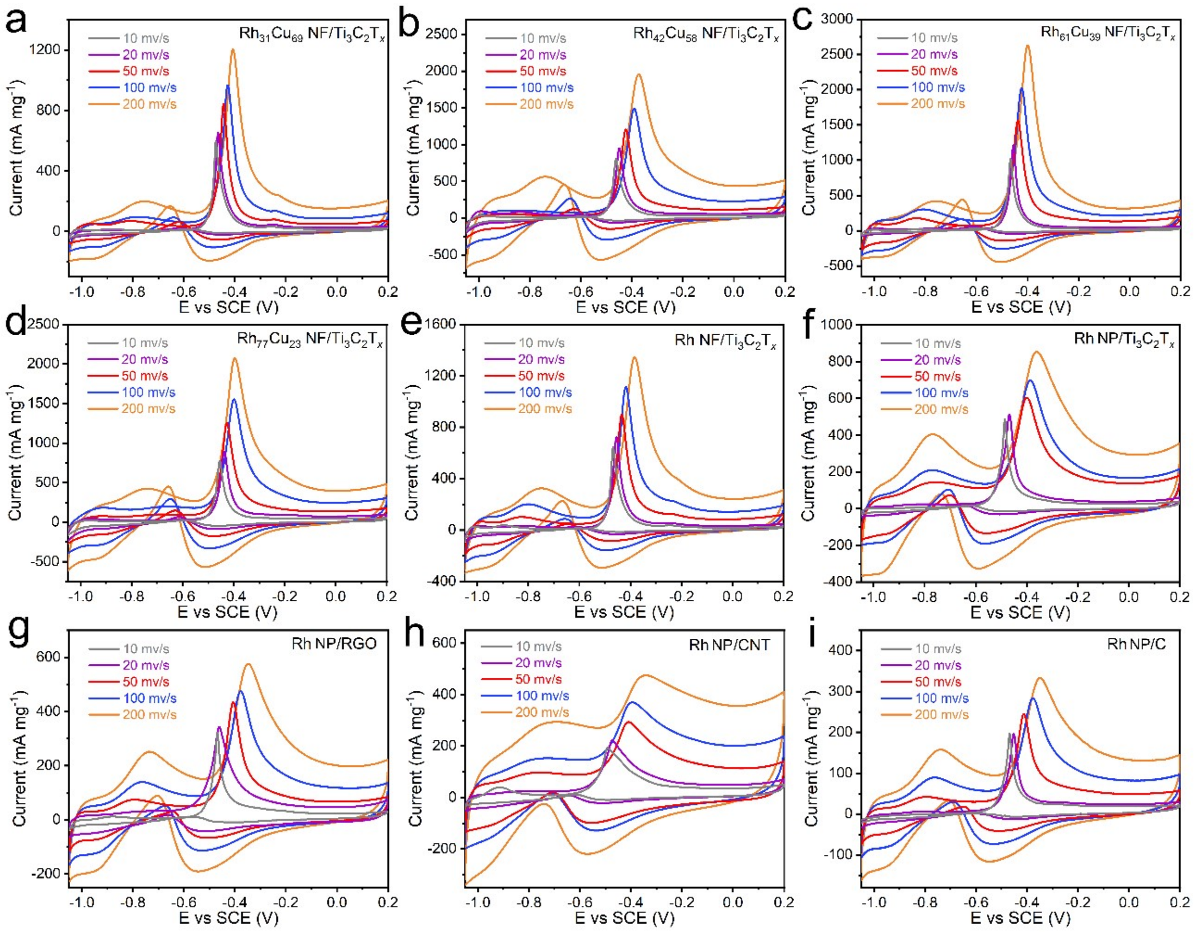

Fig. S11 The corresponding mass activities curves of (a-e) RhCu NF/$Ti_3C_2T_x$ catalysts with different Rh/Cu ratios and (f-i) Rh NP/$Ti_3C_2T_x$, Rh NP/RGO, Rh NP/CNT and Rh NP/C.

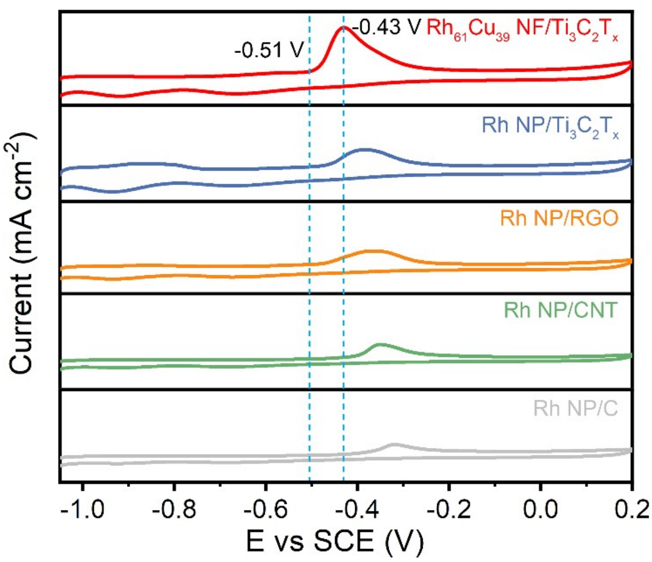

Fig. S12 CO stripping voltammograms for the $Rh_{61}Cu_{39}$ NF/$Ti_3C_2T_x$, Rh NP/$Ti_3C_2T_x$, Rh NP/RGO, Rh NP/CNT and Rh NP/C catalysts tested in 1 M KOH solution at 50 mV s^{-1}.

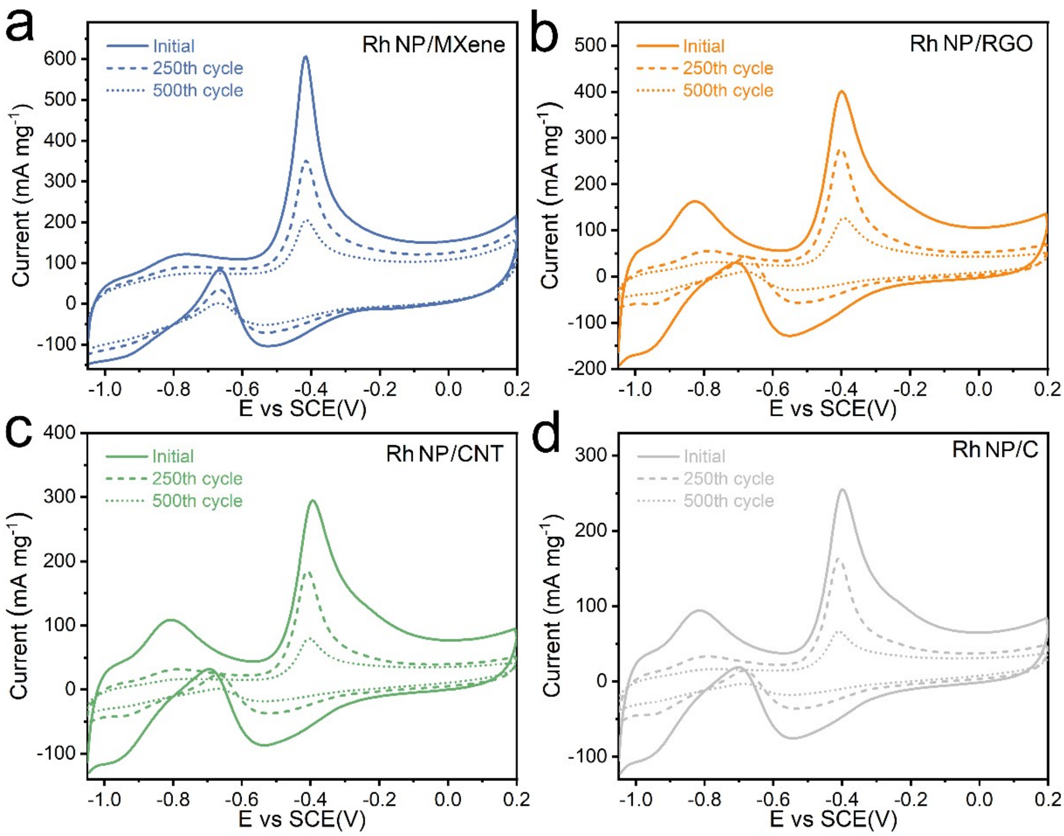

Fig. S13 The CV curves of (a) Rh NP/$Ti_3C_2T_x$, (b) Rh NP/RGO, (c) Rh NP/CNT and (d) Rh NP/C before and after 500 cycles.

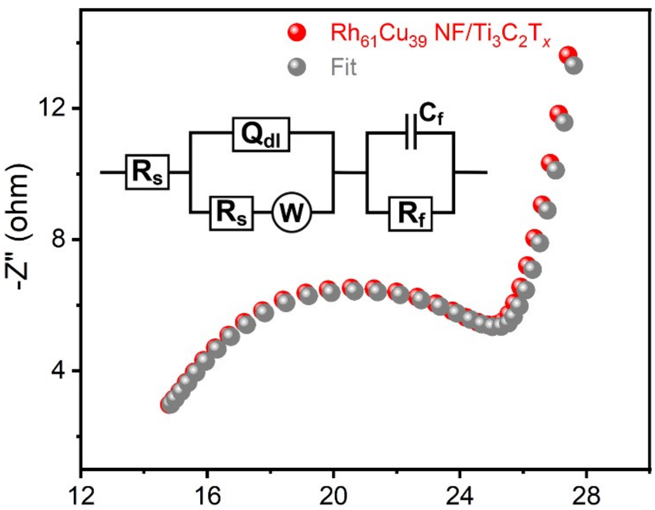

Fig. S14 Nyquist plots of EIS and fitting curve of the $Rh_{61}Cu_{39}$ NF/$Ti_3C_2T_x$ electrode.

Table S1. Summary of ICP-MS analysis for different RhCu NF/$Ti_3C_2T_x$ catalysts.

Catalysts	Rh (wt.%)	Cu (wt.%)	Rh/Cu atomic ratio
$Rh_{31}Cu_{69}$ NF/$Ti_3C_2T_x$	8.04	11.05	31 : 69
$Rh_{42}Cu_{58}$ NF/$Ti_3C_2T_x$	10.48	8.94	42 : 58
$Rh_{61}Cu_{39}$ NF/$Ti_3C_2T_x$	13.50	5.33	61 : 39
$Rh_{77}Cu_{23}$ NF/$Ti_3C_2T_x$	14.23	5.25	77 : 23

Table S2. Compiled study comparing CV results for different catalysts.

Electrode	ECSA (m^2 g^{-1})	Mass activity (mA mg^{-1})	Specific activity (mA cm^{-2})
$Rh_{31}Cu_{69}$ NF/$Ti_3C_2T_x$	78.1	822.1	1.05
$Rh_{42}Cu_{58}$ NF/$Ti_3C_2T_x$	95.3	1190.2	1.25
$Rh_{61}Cu_{39}$ NF/$Ti_3C_2T_x$	111.3	1583.0	1.42
$Rh_{77}Cu_{23}$ NF/$Ti_3C_2T_x$	97.9	1234.6	1.26
Rh NF/$Ti_3C_2T_x$	85.2	900.5	1.06
Rh NP/$Ti_3C_2T_x$	71.2	596.6	0.84
Rh NP/RGO	57.8	408.2	0.71
Rh NP/CNT	50.2	296.1	0.59
Rh NP/C	45.1	241.4	0.54

Table S3. Comparison of methanol oxidation behavior for the $Rh_{61}Cu_{39}$ NF/$Ti_3C_2T_x$ catalyst and various state-of-the-art Rh-based electrocatalysts.

Electrode	ECSA (m^2 g^{-1})	Mass activity (mA mg^{-1})	Electrolyte	Ref.
$Rh_{61}Cu_{39}$ NF/$Ti_3C_2T_x$	111.3	1583.0	1 mol L^{-1} KOH+ 1 mol L^{-1} CH_3OH	This work
Rh-NSs/RGO	48.66	264	1 mol L^{-1} KOH+ 1 mol L^{-1} CH_3OH	[S1]
Rh/MoS_2-RGO	95.5	1502	1 mol L^{-1} KOH+ 1 mol L^{-1} CH_3OH	[S2]
Rh/CNT-RGO	123.8	1228.5	1 mol L^{-1} KOH+ 1 mol L^{-1} CH_3OH	[S3]
Rh/carbon nanohorns	102.5	784.0	1 mol L^{-1} KOH+ 1 mol L^{-1} CH_3OH	[S4]
Rh nanosheets	73.17	333	1 mol L^{-1} KOH+ 0.5 mol L^{-1} CH_3OH	[S5]
Rh nanotubes	60.9	325	1 mol L^{-1} KOH+ 1 mol L^{-1} CH_3OH	[S6]
Hollow Rh spheres	50.7	292	1 mol L^{-1} KOH+ 1 mol L^{-1} CH_3OH	[S7]
Rh nanodendrites	43.35	255.6	1 mol L^{-1} KOH+ 1 mol L^{-1} CH_3OH	[S8]

Table S4. The charge-transfer resistances (R_{ct}) of different electrodes.

Electrode	R_{ct}	
	Value (ohm)	Error (%)
$Rh_{61}Cu_{39}$ NF/$Ti_3C_2T_x$	12.8	1.2
Rh NP/$Ti_3C_2T_x$	16.7	1.5
Rh NP/RGO	18.5	2.6
Rh NP/CNT	26.4	2.7
Rh NP/C	6300.5	3.9

Reference

[S1] Y. Kang, Q. Xue, P. Jin, J. Jiang, J. Zeng, Y. Chen, Rhodium nanosheets-reduced graphene oxide hybrids: a highly active platinum-alternative electrocatalyst for the methanol oxidation reaction in alkaline media, *ACS Sustainable Chem. Eng.*, 2017, **5**, 10156-10162.

[S2] Q. Zhang, Y. Li, H. He, H. Huang, Building 3D interconnected MoS_2 nanosheet-graphene networks decorated with Rh nanoparticles for boosted methanol oxidation reaction, *ACS Sustainable Chem. Eng.*, 2022, **10**, 8940-8948.

[S3] Y. Li, Y. Chen, J. Qin, J. Chen, Y. Zhao, Y. Xie, H. He, H. Huang, Three-dimensional porous low-defect carbon nanotube and graphene network supported Rh nanocrystals as efficient methanol oxidation electrocatalysts, *ChemNanoMat*, 2022, **8**, e202200176.

[S4] X. Guo, Q. Zhang, Y. Li, Y. Chen, L. Yang, H. He, X. Xu, H. Huang, Nanosized Rh grown on single-walled carbon nanohorns for efficient methanol oxidation reaction, *Rare Met.*, 2022, **41**, 2108-2117.

[S5] J. Zhu, S. Chen, Q. Xue, F. Li, H. Yao, L. Xu, Y. Chen, Hierarchical porous Rh nanosheets for methanol oxidation reaction, *Appl. Catal. B. Environ.*, 2020, **264**, 118520.

[S6] S. Wang, S. Liu, Z. Wang, Z. Dai, H. Yu, Y. Xu, X. Li, L. Wang, H. Wang, Mesoporous Rh nanotubes for efficient electro-oxidation of methanol, *J. Mater. Chem. A*, 2021, **9**, 4744-4750.

[S7] Y. Kang, Q. Xue, Y. Zhao, X. Li, P. Jin, Y. Chen, Selective etching induced synthesis of hollow Rh nanospheres electrocatalyst for alcohol oxidation reactions, *Small*, 2018, **18**, e1801239.

[S8] Y. Kang, F. Li, S. Li, P. Jin, J. Zeng, J. Jiang, Y. Chen, Unexpected catalytic activity of rhodium nanodendrites with nanosheet subunits for methanol electrooxidation in an alkaline medium, *Nano Res.*, 2016, **9**, 3893-3902.